RESEARCH ARTICLE

**Editorial Process:** Submission:03/10/2025 Acceptance:08/20/2025 Published:08/30/2025

# Green Synthesis of Silver Nanoparticles Using the Seeds of *Lupinus luteus*: Characterization and Assessment the Antibacterial and Anticancer Activities

**Noor H. Faisal[1], Nuha A. M. Obaid[1], Nuha W. Ali[1], Ali A. A. Al-Shawi[1]*, Ruaa G. Ibrahim[1], Ayat N. Hassan[1], Ayat J. Kadhum[1], Osama A. Mohsein[2,3], Iman N Luaibi[4]**

## Abstract

**Objective:** This study aimed to synthesize silver nanoparticles using the aqueous seed extract of Lupinus luteus via a green synthesis approach, and to evaluate their antibacterial and anticancer activities against liver and breast cancer cell lines. **Materials and methods:** silver nanoparticles (AgNPs) were synthesized using essential extracts from Lupinus luteus. The AgNPs were subsequently characterized using ultraviolet – visible spectroscopy, scanning electron microscopy, and Fourier transform infrared spectroscopy. The biological activities of AgNPs were examined. **Results:** The present study indicates that silver nanoparticles produced of Lupinus luteus extracts show an absorption peak at 420 nm, thereby confirming their successful synthesis. A study using scanning electron microscopy (SEM) showed that the nanoparticles' average diameter is 24.72 nm. The biological activities of these nanoparticles were examined, including their antibacterial and anticancer capabilities. Assays include flow cytometry, half-maximal inhibitory concentration (IC50), and minimum inhibitory concentration (MIC) were used in the biological activity evaluation. The nanoparticles caused cell cycle arrest at the S-phase in two human cancer cell lines, HepG2 and MCF-7. **Conclusion:** These results demonstrate how Lupinus luteus nanoparticles may be used to create cutting-edge antibacterial and anticancer treatments. Therefore, merit investigation request to develop it functions.

**Keywords:** Lupinus luteus- silver nanoparticles- antibacterial- anticancer

*Asian Pac J Cancer Prev,* **26 (9)**, 3405-3414

## Introduction

Nanotechnology is playing an essential function in many important fields like chemistry, medicine, physics, biotechnology and materials science especially nanoparticles (NPs) was one of the early development stages of nanotechnology [1]. Any materials with at least one dimension between 1 and 100 nm are referred for being an (NP) in terms of their size and morphology nanoparticles are solid atomic or molecular particles that have superior physical properties to bulk molecules [2]. Due to their ahigh surface to volume ratio and good dispersion in solution, with the ability to handle the majority of the world's health issues. Among the nanomaterials that have been widely employed in the biological areas are metallic nanoparticles (MNPs) [3]. There are three layers that make up NPs: the shell layer, which is chemically and physically different from the core; the surface layer, which can be maintained with different chemicals, metal ions, emulsifiers, and polymers; and the core, which may be the main part of the NPs. This is because NPs are not made up of simple molecules. Help treat both contagious and long-term illnesses. MNPs have better physiochemical traits than other nanoparticles because they are stronger and can do more [4]. Several metals, including copper, zinc, iron, silver, gold, palladium, platinum, and metal oxides, are used to create MNPs. Many researchers are interested in the creation of silver nanoparticles (Ag -NPs) due to its wide array of antibacterial and therapeutic features. It has been used in medicine to treat many kinds of disease since ancient times [2] it is well recognized fact that silver ions and silver-based compounds have a great microbial killing capacity [5]. However, developments in technology and deeper comprehension of how silver works to prevent disease by killing microbes have created possible its application

*[1]Department of Chemistry, College of Education for Pure Sciences, University of Basrah, Basrah, Iraq. [2]Department of Medical Laboratory Techniques, Mazaya University College, Thi-Qar, Iraq. [3]Thi-Qar Health Directorate, Al Habbobi Teaching Hospital, Thi-Qar, Iraq. [4]Department of Basic Sciences, College of Dentistry, University of Basrah, Basrah, Iraq. *For Correspondence: ali.abdulhussein@uobasrah.edu.iq*

in medicine and significantly improved physicochemical characteristics such as optical, thermal, electrical, and catalytic qualities in compared to the bulk material [6]. Researchers turned to the environmentally, friendly, and convenient synthesis of nanoparticles utilizing either animal metabolites, bacteria, fungus, algae, or plants. due to the main disadvantage of using chemical agents: their possible toxicity [7]. Routes involving plants, particularly medicinal plants, have additional benefits and don't call for complicated procedures or approaches [8]. Additionally, the plant-based method is quite simple to scale up for large-scale production of nanoscale particles. In ecological synthesis technique using plant components including leaves, stems, roots, and bark,

Combined with the necessary metal solution, such as silver nitrate, are flowers, and fruits [9]. An ancient leguminous plant known as lupin lutes has been domesticated and used as food by humans and animals for around 2000 years In the Middle East and Africa, lupin seeds (LS) are used in traditional medicine as an anti-diabetic agent [10]. There are about 300 species in the genus Lupinus, which is a member of the Fabaceae family of legumes. Because traditional lupine species have an enormous quantity of alkaloids (between 1 and 3% of the dry weight of their seeds) [11, 12]. Legumes' chemical constitution, which includes their protein level and amino acid composition, determines their feed and nutritional value. Lupine seeds were collected from herbarium in Basrah, lupin are yellow legume seeds, they are traditionally eaten as snack food, especially in the Mediterranean basin, Latin America and north Africa its used in Egypt [13]. The aim of study was to synthesis silver nanoparticles from Lupinus luteus extracts and evaluate their antibacterial and anticancer properties for possible perspective researches.

## Materials and Methods

Silver nitrate (AgNO3) was purchased from Merck Germany, lupin luteus seeds was collected from local market. Two hundred grams of lupin luteus seeds were washed with filtered water and then dried in the shade. Ten grams of the seeds were then ground into a powder using a grinder. This powder was added to a 250 ml flask in 100 ml of distilled water and incubate in oven 80 °C for two hours. This plant extract was poured out, filtered through Whatman paper, and then put in the fridge to be used later at 4 °C. 50 ml of 1M AgNO3 was slowly added to 5 ml of the extract from the seeds. The reaction was actively carried out inside the flask using a magnetic stirrer on a hot plate (60 °C). The biosynthetic reaction started around 40 minutes, and the color changed from light yellow to brown as Ag+ was broken down into shiny silver Ag0 nanoparticles. The sample was spun at 25,000 x for 15 minutes to make a pellet that was used for analysis. The seeds' extract was used for analysis; it was used as a reducing agent, a stabilizing agent, and a capping agent to synthesis the nanoparticles.

*Characterization of $AgNO_3$*

The most straight forward way to monitor AgNPs synthesis is by observing the change in color of the solution from yellow to brown before using a specific procedure for its intended application. The size, morphology and composition of nanoparticles can be examined using UV-Vis FTIR, TEM, SEM, XRD analysis is avital method a detecting nanoparticles information microscopy [14-16].

*UV spectra*

UV-visible spectroscopy is the method that is commonly performed. Most metal nanoparticles with sizes between 2 and 100 nm are typically measured between 300 and 800 nm in wavelength silver and gold nanoparticles are identified by spectrophotometric absorption bands in the wavelength ranges of 400–450 nm and 500–550 nm. The UV-visible spectra of the produced silver nanoparticle citral (1 mM) were determined using a Labo med Model UVD-2950 UV-VIS Double Beam PC, a scanning spectrophotometer with a resolution of 2 nm.

*Fourier -Transform Infrared Spectroscopy (FT-IR)*

Before being examined at 500–4000 cm-1 using an FT-IR spectrometer (Shimadzu, Koyoto, Japan), all AgNPs plant extracts were freeze-dried. This allowed for the classification of the biomolecules present in the plant herbal extracts that included the nanoparticles.

*TEM imaging of nanoparticles*

One of the best methods for analyzing the morphological characteristics of a single nanomaterial is transmission electron microscopy (TEM), which allows direct high-resolution picture capture of individual nanomaterials. Furthermore, TEM has a lot of potential for use in statistical analysis because pictures of many nanomaterials can be easily generated simultaneously transmission electron microscopy (TEM) has a 1000-fold higher resolution than SEM.

*SEM Scanning Electron Microscopy*

Using scanning electron microscopy, the size and form of lupine Ag NPs were confirmed. Platinum was used to sputter Ag NPs, which were subsequently uniformly placed on carbon tape-covered sample containers. SEM images were captured using the previously mentioned method in order to identify the presence of the fundamental components of the nanoparticles from the various times in the samples.

*X-ray diffraction analysis*

XRD is a common analytical technique for analyzing molecular and crystal structures, XRD can also assess crystallinity, isomorphous substitution, and particle size. It may also qualitatively identify active chemicals and qualitatively resolve various molecules. X-ray energy bounces off of particles and creates many diffraction peaks. These peaks show the crystalline lattice's physical and chemical features. XRD can be used to look at the structural features of many different types of materials, including proteins, glasses, polymers, inorganic catalysts, and superconductors. The shape of the diffraction peak is a key part of figuring out what these materials are like. The unique diffraction light source of each material can be used

to figure out what it is made of by comparing the diffracted beams to the Joint Committee on Powder Diffraction Standards (JCPDS) reference library. Bragg's rule is the most important idea in XRD. The Debye-Scherrer method was used to figure out how big the AgNPs were.

*Antibacterial evaluation of AgNPs*

These microbial strains were identified: Pseudomonas aeruginosa ATCC 27853 and Escherichia coli ATCC 25922. Minimum inhibitory concentrations (MICs) are the lowest levels of concentrations of each evaluated drug needed to limit the tested bacterium's observable development, according to the Clinical Laboratory Standard Institute (CLSI). In sterile microdilution trays filled with Mueller Hinton broth medium, each chemical was serially diluted twice at concentrations ranging from 0.003 to 4 mM. Subsequently, sterile normal saline was used to prepare bacterial suspensions of each strain, with the turbidity adjusted to meet the McFarland criterion of 0.5. The suspension was weakened in clean Mueller-Hinton broth (MHB) at a rate of 1:100 before being moved to the containers that had a series of dilutions of each part. At each dose, tests were done on 0.5 to 1106 bacterial cells. 96-well plates were kept at 37°C for a whole day. To test uniformity, comforting was used. Finally, tetracycline was used as a regular antibiotic against different types of germs, and all the tests were done three times. In clean D.W., 10 microliters of a reagent stock solution containing 4 mg/ml were added to each well. To find the MBC, 100 L of each dose of no-growth well was grown on a Nutrient agar plate at 37 °C for 24 hours. MBC To get the 18MBC concentrations, 100 L of each concentration was put on a Nutrient agar plate and left to grow at 37 °C for 24 hours. At MBC levels of 18, the lowest amounts needed to kill 99.9% of bacteria are reached [17,18].

*Anti-cancer activity*

Culture and cell lines. Human hepatocarcinoma HepG2 and human breast cancer cell line MCF7 . Gibco's RPMI-1640 media was used to cultivate the cells, which contained 10% FBS and antibiotics (100 U/ml penicillin and 100 µg/ml streptomycin). The cells were maintained at 37°C in humidified air with 5% CO2 and were passaged using phosphate-buffered saline (PBS) solution and trypsin/EDTA (Gibco). The MTT assay is used to determine the viability of MCF7 cells. The proliferation and vitality of the cells were assessed using the MTT [3-(4, 5-dimethylthiazol-2-yl)-2, 5-diphenyltetrazolium Bromide] (Sigma-Aldrich) assay. In summary, the cells (MCF7) were digested with trypsin, and subsequently extracted, adjusted to a density of $1.4 \times 10^4$ cells/well, and transplanted onto 96-well plates that contained 200 µl of fresh media per well. The cells were incubated for 24 hours. The cells were subjected to 600–7.4 µg/ml of the compounds for a full day at 37 °C and 5% $CO_2$ after forming a monolayer. The supernatant was discarded after 24 hours of incubation, and 200 µl of MTT solution (0.5 mg/ml in phosphate-buffered saline PBS) was transferred to each well. The monolayer culture remained unaltered in the original plate, and the plate was subsequently incubated at 37 °C for an additional 4 hours. In each well, 100 µl of dimethyl sulfoxide was added after the cell supernatant was collected to prepare the MTT solution. The cells were incubated at 37 °C on an agitator until the crystals were completely dissolved. The vitality of the cells was quantified by measuring absorbance at 570 nm using an ELISA reader (Model wave xs2, Bio Tek, USA). The concentration of the compounds that caused 50% of cell mortality ($IC_{50}$) was determined by utilizing the appropriate dose-response curves. The morphology of treated and untreated cancer cells was examined using optical microscope [19-21].

*Reactive oxygen species (ROS) assay*

Using the flow cytometry technique and 2′, 7′-dichlorodihydrofluorescin diacetates (DCFH2-DA) (Sigma-Aldrich), the production of ROS was quantified. This dye is readily taken up by cells and turns to 2′, 7′ dichlorodihydrofluorescin (DCFH2) by esterase, which remains inside the cells. When the cells reduce DCFH2, hydrogen peroxide or low-molecular-weight peroxides are made. This makes the highly visible 2′, 7′-dichlorofluorescein (DCF). This is the reason why the brightness level is directly related to the amount of peroxide the cells make from hydrogen. In general, the $IC_{50}$ concentration of the substance was used to treat cells ($1x10^5$ cells/well) for a duration of 12 hours. After centrifuging sterilized try cells at 1500 xg for 5 minutes, the pellet was washed for 30 minutes with 1 mL of PBS and then treated with DCFH2-DA (20 µM) while being stored in the dark. Following thirty minutes, data was collected in the FL1 channel and the fluorescence was analyzed using a flow cytometer to compare two luminescence excitations and emissions (485–495 nm and 525–530 nm).

*Cell cycle phase analysis*

The cells were treated for 24 hours at an $IC_{50}$ concentration of AgNPs, HepG2 and MCF-7 cells were centrifuged at 1500 xg for 5 minutes at 4 °C, and then they were repaired for 24 hours at 4 °C using 70% ethanol. They were then rinsed in 1 ml PBS. After the incubation period, the alcohol was removed from those cells by centrifuging them. The resultant pellet was treated with 20 g/ml of Ribonuclease A (RNAase) (Sigma-Aldrich) and a 20 g/ml solution of propidium iodide (Sigma-Aldrich), and resuspended in PBS for 30 minutes. The Flow software version 7.6.1 was utilized to manage the data and the flow cytometry analysis was utilized to identify the locations of different cell cycle stages.

*Detection of apoptosis by annexin V-FITC and PI staining*

Using the Bio Vision annexin V-FITC apoptosis kit, we were able to identify apoptotic and dead HepG2 and MCF-7 cells that had been injected with AgNPs. One day following the Ag NPs $IC_{50}$ concentration treatment, the cells were harvested, meticulously cleaned, and tagged with FITC and propidium iodide (PI). Following a 24 hour treatment with NA $IC_{50}$ concentration, $5x10^5$ cells were collected and centrifuged (1500 xg for 10 minutes) with ignored control cells. The FL3 signal detector that was to be tested was unable to detect PI-stained cells,

while the FL1 indication detector did. Following fragment recovery in 500 µl of 1X attachment buffer, 5 µl of annexin V-FITC and 5 µl of a 50 g/ml propidium iodide solution were added, and the mixture was allowed to sit at room temperature for five minutes.

*Statistical Analysis*

The graph's The excel file's amount response curve is used to compute the $IC_{50}$. In the green chart, all the absorbances at 570 nm are recorded for every concentration. The percentage of viability for each concentration is computed using the absorbances, Next, the standard deviation and average viability are determined. You may view the computations by clicking on each in the Excel c The graph's curve was created using the data in the chart, and the equation pertaining to it was computed and shown in right corner. $IC_{50}$ was computed by replacing y in the equation with 50, which denotes 50% viability, and calculating the x value at y=50 to show $IC_{50}$ concentration. To calculate the $IC_{50}$, values a and b are taken out of the equation Calculations using statistics are not relevant. in order to compute $IC_{50}$.

## Results

*FT-IR*

The FTIR spectrum of aqueous extract of Lupinus luteus with silver nanoparticles showing peaks at (3879cm -1- 3726 cm-1 corresponding to (OH stretch, H–bonded of alcohols/phenols) 2978cm-1 due to – (C-H stretching in alkanes 2311cm-1. This peak could be related to C≡C stretching or possibly C≡N stretching vibrations, 1750cm-1. This peak is commonly associated with C=O stretching vibrations in carbonyl groups. It might indicate the presence of esters, aldehydes, or ketones.1511cm-1, this peak indicates stretching vibrations from the aromatic C=C functional group. Peaks at 1394 $cm^{-1}$ and 1061 $cm^{-1}$ are indicative of C-H bending vibrations and C-O stretching, respectively, which could refer to carboxylate groups or other organic interactions [22,23], Figure 1A.

*UV spectra*

UV-visible spectrum of silver nanoparticles (AgNPs) synthesized using Lupinus luteus extract is shown in Figure 1B. The color change of the plant extract and $AgNO_3$ solution from light yellow to reddish-brown indicates the reduction of $Ag^+$ ions, confirming the formation of silver nanoparticles. The spectrum exhibits a peak at approximately 420 nm, which is attributed to the plasmon resonance of the metallic silver nanoparticles. Previous studies have reported similar plasmon resonance peaks in the UV-visible spectra of AgNPs, with absorption peaks typically observed between 350 and 450 nm. This variation in the peak position and intensity can be influenced by factors such as the size and shape of the nanoparticles present in the reaction solution [24].

*X-ray diffraction analysis (XRD)*

An advanced characterization spectroscopic technique called X-ray diffraction (XRD) analysis is used to assess the crystalline quality of biosynthesized AgNPs. XRD pattern showed three distinctive diffraction peaks according to the equivalent planes at 20.37 (111), 32.19 (200), and 63.86 (220). These peaks are consistent with the standard diffraction patterns for silver, this pattern demonstrated our synthesized nanoparticle's crystalline nature and face-centered cubic (FCC) structure [25], Figure 2.

*TEM*

To find out the size and form of the produced NPs, TEM examination is performed. The TEM images of Ag NPs synthesized using Lupinus luteus extract show mostly spherical irregular, and extremely agglomerated, with diameters ranging from 3 to 5nm. The differences in shapes and sizes were because of aggregation, Van der Waals forces frequently cause aggregation. Especially when stabilizers are either absent or insufficient. All of these elements work together to give silver nanoparticles their various forms and aggregation patterns [26], Figure 3.

*SEM*

SEM (scanning electron microscope) was used to determine the size and morphology of the synthesized Ag NPs. The Lupinus luteus -derived nanoparticle extract was examined via Scanning Electron Microscopy (SEM) at various particle sizes (500 nm, 200 nm, 1 µm, 2 µm, 5 µm, and 10 µm), with a radius of 25 nm. The results showed that Van der Waals forces cause smaller particles (500 nm and 200 nm) to congregate, resulting in a non-homogeneous distribution. On the other hand, because these forces had less of an effect on larger particles (1 µm to 10 µm), they showed more uniform dispersion and stability. This suggests that the distribution and aggregation of nanoparticles are significantly influenced by Van der Waals forces [27], Figure 3.

*The antibacterial activity of AgNPs*

The AgNPs showed a positive biocidal effect against Pseudomonas aeruginosa and Escherichia coli, which are Gram-negative bacteria. The results from the antibacterial activity tests show that the minimum inhibitory concentration (MIC) and minimum bactericidal concentration (MBC) values are the same ,The MIC and MBC values were found to be 0.125 mg/mL for *P. aeruginosa* and 0.0625 mg/mL for *E. coli*, Table 1. Suggesting that the concentration required to inhibit bacterial growth is also sufficient to kill the bacteria, which aligns with findings from previous study [28]. Previous research has shown that the antibacterial properties of AgNPs are significantly influenced by the size and morphology of the silver particles. Smaller particles tend to have enhanced antibacterial properties due to increased surface area, which leads to a higher rate of silver ion release and more effective microbial inhibition. The release of silver ions is the primary mechanism responsible for the antibacterial effects of AgNPs. Other mechanisms include cellular membrane disruption, the generation of reactive oxygen species (ROS), and direct interaction with cellular components such as DNA and ATP. Studies have documented that silver ions can damage

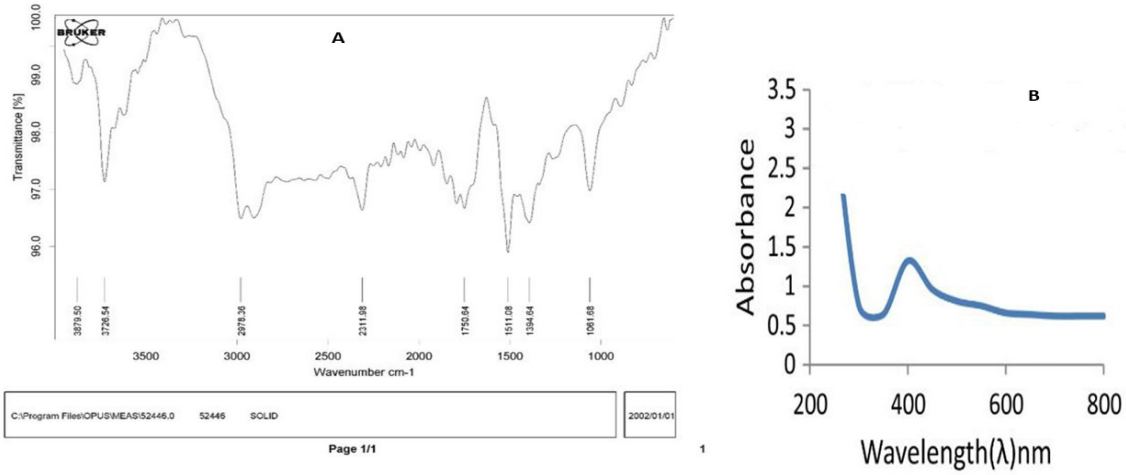


Figure 1. Display A: FT-IR of AgNPs. B- UV spectra of AgNPs.

cell membranes by creating pores, which is often observed through transmission electron microscopy (TEM). Silver ions also interact with membrane proteins, particularly those containing sulfur groups, leading to physical damage to the bacterial membrane [29, 30].

*Anticancer activity*

The anticancer property of AgNPs was assessed against MCF7 and HepG2 using a MTT cell viability assay. Both kinds of cancer cell were treated with different concentration of AgNPs (7.4, 22.22, 66.66, 200, 600) µg/ml. Silver nanoparticles using lupin seeds extract were showed more significant cytotoxic activity. Greater cytotoxic effect was observed at 600 µg/ml for both, and the $IC_{50}$ value were 236 µg/ml for MCF7 and 219 µg/ml for HepG2, Figure 4. Because AgNPs have a significant cytotoxic effect on malignant cell lines but a lower toxicity on normal cell lines [31]. They have garnered significant attention recently about their potential application as an anticancer therapeutic agent. Consistent with previous research on the dose-dependent cytotoxicity of nanoparticles, our results highlight the significant lethal effects of higher concentrations of silver nanoparticles (AgNPs) [32]. The study demonstrates that AgNPs exert a concentration-dependent impact on cell viability. Specifically, we observed a notable decrease in cell viability at elevated AgNP concentrations, which aligns with the current understanding of nanoparticle toxicity patterns. Ag+ produced by AgNPs may bind directly to RNA polymerase and inhibit its activity, according to certain theories [33]. The production of reactive oxygen species (ROS), which causes intracellular oxidative stress and ultimately cell death, is another important explanation for cytotoxicity. It has been noted that AgNPs' cytotoxicity varies with their size.

AgNPs which are smaller in size have an easier time piercing the cell membrane and interacting with various cell components. Furthermore, AgNPs with larger surface areas have reportedly been shown to be able to sustainably release more silver [34, 35]. In addition, Figures 5 and 6 were shown the changes of MCF7 and HepG2 cells morphology with the varies concentrations (7.4, 22.22, 66.66, 200, 600) µg/ml, which affected cells growth, as compared with control (untreated cells) Figures 5A and

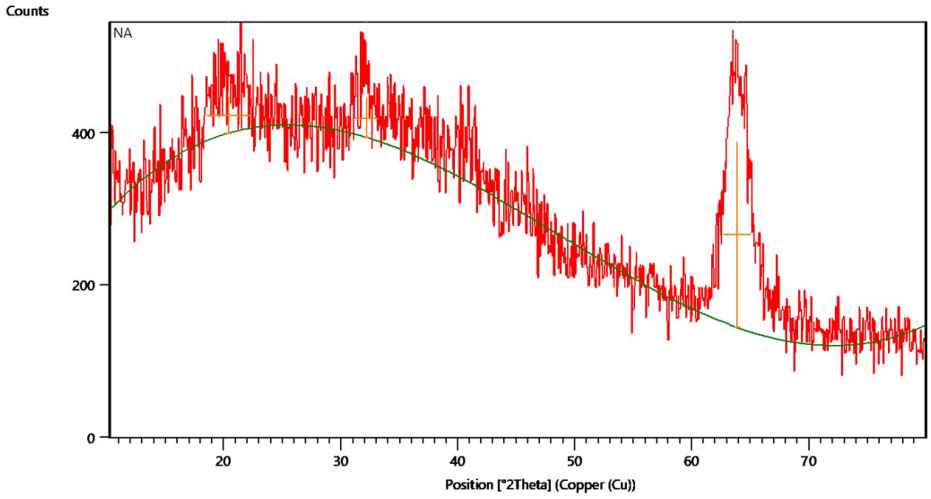


Figure 2. XRD of AgNPs

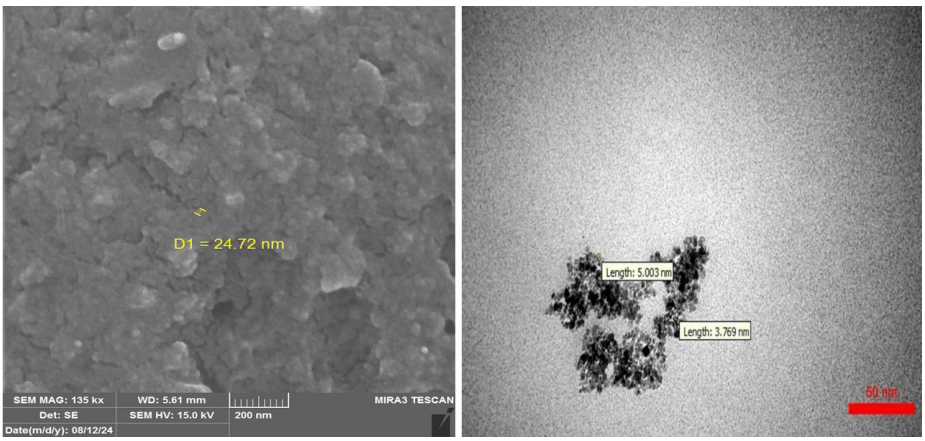


Figure 3. SEM and TEM of AgNPs

Supplementary Figure 1A.

## Discussion

*Cell cycle analysis*

Cell cycle analysis of HepG2 liver cancer cells and MCF7 breast cancer cells treated with the $IC_{50}$ concentration of the plant extract-derived silver nanoparticles AgNPs revealed significant disruptions in cell cycle progression. Flow cytometric analysis demonstrated substantial changes in cell cycle distribution compared to control cells [36]. Notably, a marked increase in the percentage of cells in the Sub-G1 phase, indicating DNA fragmentation and apoptosis, was observed. Specifically, 49.8% of MCF7 cells and 21.4% of HepG2 cells were in the Sub-G1 phase after treatment, compared to only 15.5% and 17.2% in untreated control cells, respectively. In addition, an accumulation of cells in the S phase was observed, with 20% of MCF7 cells and 38.3% of HepG2 cells, suggesting that the extract impairs DNA synthesis progression by delaying phase transitions or inducing replication stress. In contrast, normal cell cycle progression in control cells showed 12.7% of MCF7 cells and 15.5% of HepG2 cells in the S phase. Control cells also exhibited a balanced distribution with a higher proportion of cells in the G1 and G2/M phases, indicative of regular cell division and cycle progression. Specifically, 28.5% of HepG2 and 28.5% of MCF7 cells were in the G2/M phase, while 40.5% of HepG2 and 43.3% of MCF7 cells were in the G1 phase, Supplementary Figure 2. Treatment with the

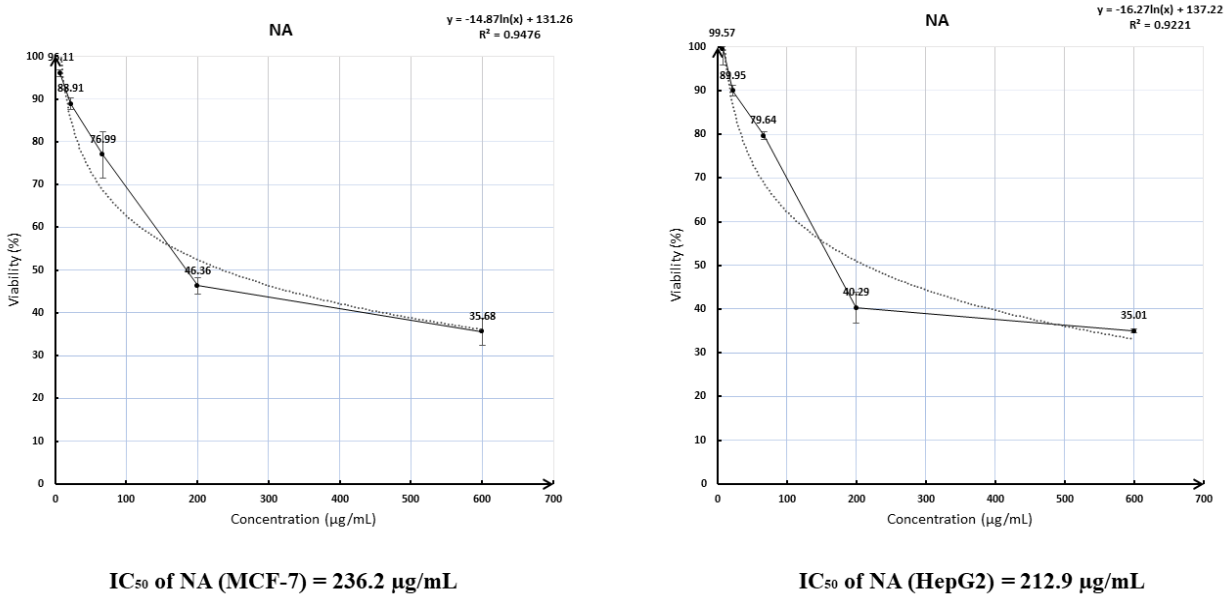


Figure 4. $IC_{50}$ Values of AgNPs against MCF7 and HepG2 Cancer Cells

Table 1. MIC and MBC Values of AgNPs against *Pseudomonas aeruginosa* ATT10145 and Escherichia coli ATCC1399

| Sample | Pseudomonas aeruginosa ATT10145 | | Escherichia coli ATCC1399 | |
|---|---|---|---|---|
| | MIC (mg/ml) | MBC (mg/ml) | MIC (mg/ml) | MBC (mg/ml) |
| AgNPs | 0.125 | 0.125 | 0.0625 | 0.0625 |

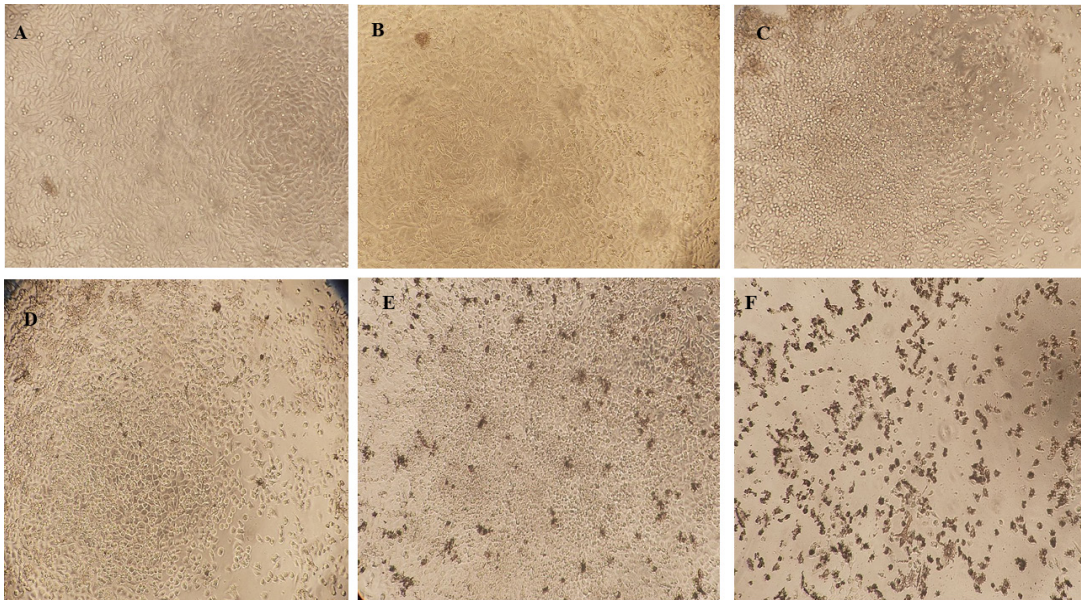


Figure 5. Showed the Effect of $IC_{50}$ Values of AgNPs on the Morphology Changes of MCF7 Cancer Cells

extract significantly reduced the cell population in both the G1 and G2/M phases, likely due to apoptotic signaling pathways and cell cycle arrest. This disruption in normal cell cycle progression underscores the extract's dual anti-cancer effects: apoptosis induction and inhibition of cell proliferation through DNA replication arrest. The findings provide strong evidence of a specific mechanism involving both S-phase arrest and apoptosis induction, supporting the potential therapeutic application of the plant extract as a cytotoxic agent targeting proliferative pathways in cancer cells [37,38].

*Apoptosis*

To assess and contrast the efficacy of AgNPs against HepG2 cells and MCF7 cells, we used an apoptotic assay. In eukaryotes like humans, apoptosis is a type of planned cell death. It has been documented in bacterial apoptotic processes and both unicellular and multicellular eukaryotes. As the inner mitochondrial transmembrane potential collapses during apoptosis, membrane permeability changes [39]. The following stage is distinguished by nuclear fragmentation and chromatin condensation. In order to reduce inflammation, the cell then splits into membrane-bound, ultra-structurally maintained fragments that macrophages eat. Plotting the forward and side scatter densities will help you locate your target cell population and eliminate waste [40].

To find cells that are interesting based on size and detail (complexities), FSC vs. SSC gating was employed. While side scatter represents the granularity or intricacy of the cell, forward scatter is often thought to represent the size of the cell. The cell population in treated and untreated cells was chosen for additional study using the SSC VS FSC plot. The condition of the cell population that was gated using the FSC vs. SSC plot is displayed in the FL1 vs. FL3 plot. Hence, there are four quartiles in the FL1 versus FL3 graphic. The cell population that is not stained with FITC-conjugated annexin or PI is displayed in the Q4 quartile. The Q4 quartile displays healthy cells that are neither necrotic nor apoptotic. The cell population that is exclusively stained with FITC-conjugated annexin and is thus in the early phases of apoptosis is displayed in the Q3 quartile [41]. Since the integrity of the cell membrane is not threatened during the early phases of apoptosis, PI stain is not allowed to enter the cells. FITC-conjugated annexin, on the other hand, attaches itself to phosphatidylserines found in the cytoplasmic membrane's outer layer. The Q2 quartile denotes the cell population stained with both PI and FITC-conjugated annexin, indicating cells in the late stage of apoptosis, characterized by compromised cell membrane integrity, allowing PI to permeate the cell and stain the DNA, while phosphatidylserine is externalized to bind with annexin [42]. The Q1 quartile contains necrotic cells. The necrotic cell's plasma membrane is ruptured, and PI stain may easily penetrate the cells, thereby removing debris and artifacts from the study. The $IC_{50}$ value was used to quantify early apoptosis (Q1), late apoptosis (Q2), necrosis (Q3), and cell survival (Q4). Untreated HepG2 cells exhibited early apoptosis (0.329%), late apoptosis (0.674%), necrosis (0.303%), and live cells (98. 7%), as illustrated in Supplementary Figure 3A. HepG2 cells treated with $IC_{50}$ demonstrated early apoptosis (0.4%), late apoptosis (0.090%), necrosis (65.0 1%), and viable cells (34.5%) Supplementary Figure 3B. Supplementary Figure 3C shows untreated MCF7 cells in early apoptosis (6.89%), late apoptosis (3.53%), necrosis (3.09%), and surviving cells (86.48%). The efficacy of apoptosis in MCF7 cells revealed early apoptosis (0.25%), late apoptosis (5.14%), necrosis (33.19%), and live cells (61.42.6%), Supplementary Figure 3D [43].

*ROS*

Using flow cytometry, the ROS data were evaluated using the $IC_{50}$ values. DCFH is employed as a ROS biomarker by contrasting treated and untreated cells. This dye may identify several ROS activities in cells, including peroxyl and hydroxyl radicals [44]. It is changed into a

nonfluorescent molecule by cellular esterases, and ROS then oxidizes it to create 2′, 7′-dichlorofluorescein (DCF). Since ROS contributes to cell deterioration. DCFH is a crucial technique for measuring ROS levels in treated cells and comparing them to untreated cells to assess the effectiveness of drugs or plant extracts, despite the fact that it is readily impacted by light irradiation during measurements [45]. Supplementary Figure 4, illustrates that untreated (control MCF7 cells have (11.99%) DCFH+ and cells treated with AgNFs $IC_{50}$ values have27.61%) DCFH+.

Supplementary Figure 5, Untreated HepG2 cells (control) had 27.16% DCFH+, whereas cells treated with the $IC_{50}$ value of AgNFs had 41.84% DCFH+. The ROS production is interpreted using the count-FL1 plot. The FL1 peak has moved to the right in the treated cells in contrast to the control cells. An increase in ROS generation is related to the amount of fluorescent light produced by the cell population, which increases as the peak moves to the right [46].

Due to resource constraints and methodological limitations, this study was limited in that it did not include control groups to compare chemically generated silver nanoparticles to the plant extract alone. However, a previous study shown that the extract from Lupinus luteus had antioxidant and antibacterial properties when used alone, implying a possible synergistic impact between the plant extract and silver nanoparticles in increasing bioactivity [47]. Numerous studies have underlined the role of bioactive phytochemicals in green synthesis, which function as both biological efficacy boosters and reducing agents. This adds credibility to the notion that the plant extract and silver nanoparticles acting together can create the antibacterial effects shown in this study [48-49].

In conclusion, the Lupinus luteus can effectively engage in the formation of AgNPs, which verified by FT-IR, SEM, and UV analysis. The AgNPs exhibited antibacterial action against *E. coli* and *P. aeruginosa*. AgNPs displayed anticancer potential in HepG2 and MCF7 cells. Based on the anticancer investigation, AgNPs of Lupinus luteus may be created in the future to protect against a variety of diseases. Lupinus luteus might be deemed an acceptable element for the creation of AgNps, and this method could potentially be employed to produce these AgNPs in an environmentally beneficial manner.

## Author Contribution Statement

AAA and NHF were contributed in designing, analysis, and writing the manuscript; NAMO, NWA, RGI, ANH, OAM, AJK, and INL were contributed in the experiments of synthesis and analysis. All authors were approved the final version of manuscript

## Acknowledgements

None.

*Ethical approval*

This research is approved by the ethical committee at Department of Chemistry, College of Education for Pure Sciences, University of Basrah.

*Conflict of interest*

The authors declare there is no conflict of interest

## References

1.Nangare SN, Patil PO. Green Synthesis of Silver Nanoparticles: An Eco-Friendly Approach. Nano Biomed Eng. 2020;12(4): 281-96. https://doi.org/10.5101/nbe.v12i4.

2.Khan Y, Sadia H , Ali Shah SZ, Khan MN, Shah A, UllahKhedher N , et.al. Classification, Synthetic, and Characterization Approaches to Nanoparticles, and Their Applications in Various Fields of nanotechnology :A Review. Catalysts .2022;12(11). https://doi.org/10.3390/catal12111386.

3.Bhardwaj L, Rath P, Choudhury M. A Comprehensive Review on the Classification, Uses, Sources of Nanoparticles (NPs) and Their Toxicity on Health. Aerosol Sci Eng. 2023;7:69–86. https://doi.org/10.1007/s41810-022-00163-4.

4.Ratan ZA , Haidere MF, Nurunnabi M, Shahriar SM, Ahammad AJ, Shim Y, et al. Green chemistry synthesis of silver nanoparticles and their potential anticancer effects. Cancers. 2020;12(4):855. https://doi.org/10.3390/cancers12040855.

5.Xia Y, Yang P, Sun Y, Wu Y, Mayers B, Gates B, et al. One-Dimensional Nanostructures: Synthesis, Characterization, and Applications. Adv Mater .2003;15(5):353-389. https://doi.org/10.1002/adma.200390087.

6.Joudeh N, Linke D. Nanoparticle classification, physicochemical properties, characterization, and applications: a comprehensive review for biologists. J Nanobiotechnol. 2022;20(1). https://doi.org/10.1186/s12951-022-01477-8.

7.Xu JJ , Zhang W, Guo YW , Chen XY, Zhang YN. Metal nanoparticles as a promising technology in targeted cancer treatment. Drug Deliv.2022;29(1):664–678. https://doi.org/10.1080/10717544.2022.2039804.

8.Simon S, Sibuyi NR, Fadaka AO, Meyer S , Josephs J , Onani MO, et al. Biomedical Applications of Plant Extract-Synthesized Silver Nanoparticles. Biomedicines .2022;10(11):2792. https://doi.org/10.3390/biomedicines10112792xv 5t3.

9.Habeeb RHB , Dhandapani R , Narayanan S, Palanivel V, Paramasivam R, Subbarayalu R ,et al. Medicinal plants mediated the green synthesis of silver nanoparticles and their biomedical applications. IET Nanobiotechnol. 2022;16(4):115–44. https://doi.org/10.1049/nbt2.12078.

10.Mahdavi Z, Rezvani H, Keshavarz M, Moraveji M. Core-shell nanoparticles used in drug delivery-microfluidics: a review. RSC Adv. 2020;10(31):18280–95. https://doi.org/10.1039/D0RA01032D.

11.Lee SH, Jun BH. Silver nanoparticles: Synthesis and application for nanomedicine. Int J Mol Sci. 2019;20(4):865. https://doi.org/10.3390/ijms20040865.

12.Al-Shawi AAA, Hameed MF, Hussein KA, Neamah HF, Luaibi IN. Gas Chromatography-Mass Spectrometry Analysis of Bioactive Compounds of Iraqi Truffle Terfezia claveryi (Ascomycetes), Synthesis of Silver Nanoparticles, and Appraisal of Its Biological Activities. Int J Med Mushrooms. 2021;23(3):79-89. https://doi.org/10.1615/intjmedmushrooms.2021037706.

13.Chandrakala V, Aruna V, Angajala G. Review on metal nanoparticles as nanocarriers: current challenges and perspectives in drug delivery systems. Emergent Mat. 2022;5:1593–615. https://doi.org/10.1007/s42247-021-00335.

14.Thawini HK, Al-Shawi AAA. A polysaccharide of Ziziphus spina-Christi L., and it's Silver nanoparticles induced

reactive oxygen species and late apoptosis of Liver cancer cells. Nanomedicine J. 2021;6(3):37–47. https://doi.org/10.22034/nmrj.2021.03.004.

15.Raheem MA, Abdulnabi ZA , Al-Shawi AAA. Synthesis and Characterization of Multiwalled Carbon Nanotubes Decorated by ZnO and Ag2O for Using to Remove Methyl Green and Erythrosin B Dyes from Their Aqueous Solutions. Ann Chim-Sci Mat. 2025;49(1):83-93. https://doi.org/10.18280/acsm.490111.

16.Al-Shawi AAA , Hameed MF, Ali H , Hussein KA. Investigations of Phytoconstituents, Antioxidant and Anti-Liver Cancer Activities of Saueda monoica Forssk Extracted by Microwave-Assisted Extraction. Asian Pac J Cancer Prev. 2020;21(8):2349-55. https://doi.org/10.31557/apjcp.2020.21.8.2349.

17.Albakhit SDY, Mutlaq DZ ,Al- Shawi AAA. Antibacterial, Antifungal, and Antitumor Properties of 2,5-Pyrrolidinedione Derivatives. Chemistry Africa. 2023;26:2933–44. https://doi.org/10.1007/s42250-023-00710-7.

18.Kalefa N, Al-Shawi AAA. The essential oils isolated from the fruit of Ficus carica induced reactive oxygen species and apoptosis of human liver cancer cells. Egypt J Chem. 2023;2:257-65. https://doi.org/10.21608/ejchem.2022.136132.5995.

19.AbdulJabar LA, Al-Shawi AAA, Mutlaq DZ. Anti-liver and anti-breast cancer activities of 2-thioxo-4-imidazolidinone derivatives. Med Chem Res. 2021;30:43–50. https://doi.org/10.21203/rs.3.rs-488343/v1.

20.Hameed F, Mkashaf IA, Al-Shawi AAA, Hussein KA. Antioxidant and anticancer activities of heart components extracted from Iraqi Phoenix dactylifera chick. Asian Pac J Cancer Prev. 2021;11:3533–41. https://doi.org/10.31557/APJCP.2021.22.11.3533.

21.Kebede G, Feyissa Faji F, Mohammed K, Geleti D, Assefa G, Dejene M, et al. Effects of variety and seeding rate on performance of sweet lupin (Lupinus angustifolius) at Holetta, in the Central Highlands of Ethiopia. OMO Int J Sci Arba Minch Univ. 2023;6:12–35. https://doi.org/10.59122/13439LQ

22.Boukid F, Pasqualone A. Lupine (Lupinus spp.) proteins: characteristics, safety and food applications. Eur Food Res Technol. 2022;248:345–56. https://doi.org/10.1007%2Fs00217-021-03909-5.

23.Yeheyis L, Mekonnen W. New sweet blue lupin, Lupinus angustifolius L. varieties (Sanabor and Vitabor) for Ethiopia. Ethiop J Sci Technol. 2022;15:167–80. https://doi.org/10.4314/ejst.v15i1.5.

24.Bartkiene E, Bartkevics V, Starkute V, Krungleviciute V, Cizeikiene D, Zadeike D, et al. Chemical composition and nutritional value of seeds of Lupinus luteus L., L. angustifolius L. and new hybrid lines of L. angustifolius L. Lith Inst Agric. 2016;103:107–14. https://doi.org/10.13080/z-a.2016.103.014

25.Praniewicz K. Chemical composition of lupin (Lupinus spp.) as influenced by variety and tillage system. Agriculture. 2022;12:1–13. https://doi.org/10.3390/agriculture12020263.

26.Grela ER, Kiczorowska B, Samolińska W, Matras J, Kiczorowski P, Rybiński W, et al. Chemical composition of leguminous seeds: part I—content of basic nutrients, amino acids, phytochemical compounds, and antioxidant activity. Eur Food Res Technol. 2017;243(8):1385–95. https://doi.org/10.1007/s00217-017-2849-7.

27.Valente IM, Sousa C, Almeida M, Miranda C, Pinheiro V, Garcia-Santos S, et al. Insights from the yield, protein production, and detailed alkaloid composition of white (lupinus albus), narrow-leafed (lupinus angustifolius), and yellow (lupinus luteus) lupin cultivars in the mediterranean region. Front Plant Sci. 2023;14:1231777. https://doi.org/10.3389/fpls.2023.1231777.

28.Cabello-Hurtado F, Keller J, Ley J, Sanchez-Lucas R, Jorrín JV, Jorrín-Novo JV. A Proteomics for exploiting diversity of lupin seed storage proteins and their use as nutraceuticals for health and welfare. J Proteomics. 2016;143:57–68. https://doi.org/10.1016/j.jprot.2016.03.026

29.Oves M, Rauf MA, Qari HA. Therapeutic Applications of Biogenic Silver Nanomaterial Synthesized from the Paper Flower of Bougainvillea glabra (Miami, Pink). Nanomaterials. 2023;13(3):615. https://doi.org/10.3390/nano13030615.

30.Pal S, Tak YK, Song JM. Does the antibacterial activity of silver nanoparticles depend on the shape of the nanoparticle? A study of the gram-negative bacterium Escherichia coli. Appl Environ Microbiol. 2007;73:1712–20. https://doi.org/10.1128/aem.02218-06.

31.Huang H, Yang X. Synthesis of polysaccharide-stabilized gold and silver nanoparticles: A green method. Carbohydr Res. 2004;399(15):2627–31. https://doi.org/10.1016/j.carres.2004.08.005.

32.Lee B, Yoon S, Lee J W, Kim Y, Chang J, Yun J. Statistical Characterization of the Morphologies of Nanoparticles through Machine Learning Based Electron Microscopy Image Analysis. ACS Nano. American Chemical Society. 2020;14(12):17125–33. https://doi.org/10.1021/acsnano.0c06809.

33.Sreelekha E, George E, Shyam A, Sajina N, Mathew B. A Comparative Study on the Synthesis, Characterization, and Antioxidant Activity of Green and Chemically Synthesized Silver Nanoparticles. J Bionanosci. 2021;11:489–96. https://doi.org/10.1007/s12668-021-00824-7.

34.Khanal L, Sharma K, Paudyal H, Parajuli K, Dahal B, Gharty Chhetri G, et al. Green synthesis of silver nanoparticles from root extracts of rubus ellipticus sm. And comparison of antioxidant and antibacterial activity. J Nanomater. 2022;2022:1-11. https://doi.org/10.1155/2022/1832587

35.Arshad H, Sami MA, Sadaf S, Hassan U. Salvadora persica mediated synthesis of silver nanoparticles and their antimicrobial efficacy. Sci Rep .2021;11(1). https://doi.org/10.1038/s41598-021-85584-w.

36.Tyagi P, Tyagi S, Gola D, Arya A, Ayatollahi SA, Alshehri M, et al. Ascorbic acid and polyphenols mediated green synthesis of silver nanoparticles from tagetes erecta l. Aqueous leaf extract and studied their antioxidant properties. J Nanomater. 2021;2021:1-9. https://doi.org/10.1155/2021/6515419

37.Tyagi K. Estimation of toxic effects of chemically and biologically synthesized silver nanoparticles on human gut microflora containing Bacillus subtilis. J Toxicol Environ Health Sci. 2013;5(9):172–7. https://doi.org/10.5897/JTEHS2013.0271.

38.Mehdi M, Al-Alawi Ah, Thabit A, Omar G, Pradhan V. Analysis of Bioactive Chemical Compounds of Leaves Extracts from Tamarindus indica Using FT-IR and GC-MS Spectroscopy. Asian J Res Biochem. 2021;8(1):22–34. https://doi.org/10.9734/AJRB/2021/v8i130171.

39.Sulistiorini M, Gusrizal G, Sapar A. Synthesis and Characterization of Silver Nanoparticles Using Bioreductant Andong Leaf Extract (Cordyline fruticosa (L) A. Chev.). J Kim Sains Apl. 2024;27(5):243–9. https://doi.org/10.14710/jksa.27.5.243-249.

40.Perera KMKG, Kuruppu KASS, Chamara AMR, Thiripuranathar G. Characterization of spherical Ag nanoparticles synthesized from the agricultural wastes of Garcinia mangostana and Nephelium lappaceum and their applications as a photo catalyzer and fluorescence quencher. SN Applied Sci. 2020;2(12). https://doi.org/10.1007/s42452-

020-03640-y.
41.Panda MK, Dhal NK, Kumar M, Mishra PM, Behera RK. Green synthesis of silver nanoparticles and its potential effect on phytopathogens. Mater Today Proc. 2021;35(2):233–8. https://doi.org/10.1016/j.matpr.2020.05.188.
42.Obaid NM , Faisal NH , Ali NW, Ibrahim RG, Hassan N, Kadhum AJ, et al. Synthesis, characterization, and biological activity of silver nanofibers essential oils of prunus dulcis. Egypt Pharm J. 2024;24:58-88. https://doi.org/10.4103/epj.epj_226_24.
43.Sabapathi N, Ramalingam S, Aruljothi KN , Lee J, Barathi S. Characterization and Therapeutic Applications of Biosynthesized Silver Nanoparticles Using Cassia auriculate Flower Extract. Plants. 2023;12(4):707. https://doi.org/10.3390/plants12040707.
44.Ahmad HS, Ateeb M, Noreen S, Farooq MI, Baig MI, Nazar MS, et al. Biomimetic synthesis and characterization of silver nanoparticles from Dipterygium glaucum extract and its anti-cancerous activities. J Mol Struct. 2023;1282. https://doi.org/10.1016/j.molstruc.2023.135196.
45.Buszewski B, Rafińska K, Cvetanović A, Walczak J, Krakowska A, Rudnicka J, Zeković Z. Phytochemical analysis and biological activity of Lupinus luteus seeds extracts obtained by supercritical fluid extraction. Phytochem Lett. 2019;30:338-48. https://doi.org/10.1016/j.phytol.2019.02.014.
46.Vanlalveni C, Lallianrawna S, Biswas A, Selvaraj M, Changmai B, Rokhum SL. Green synthesis of silver nanoparticles using plant extracts and their antimicrobial activities: a review of recent literature. RSC Adv. 2021;11(5):2804-37. https://doi.org/10.1039/d0ra09941d.
47.Kharissova OV, Dias HV, Kharisov BI, Pérez BO, Pérez VM. The greener synthesis of nanoparticles. Trends Biotechnol. 2013;31(4):240-8. https://doi.org/10.1016/j.tibtech.2013.01.003.
48.Ahmed SB, Hamed MS, Khiralla GM, Mohamed AF. Cactus and lupin extracts as prospective anticancer agents compared with utoral drug. J Food Biochem. 2020;44(8):e13299. https://doi.org/10.1111/jfbc.13299.
49.Romeo FV, Fabroni S, Ballistreri G, Muccilli S, Spina A, Rapisarda P. Characterization and Antimicrobial Activity of Alkaloid Extracts from Seeds of Different Genotypes of Lupinus spp. Sustainability. 2018;10(3):788. https://doi.org/10.3390/su10030788.